

# Linear and Non-Linear Carrier Control of Soft Switched Isolated Boost Converter for Low Voltage Fuel Cell Applications

S. Vijaya Madhavi\*, Dr. G. Tulasi Ram Das\*\*

\*Department of EEE, Research Scholar JNTU Hyd, Flat No G1 Srivari Sannidhi Aptmnts Siri Enclave Venkatraya Nagar Nizampet Hyderabad-500090

\*\*Department of EEE, Professor JNTU Hyd, Dr. G. Tulasi Ram Das Professor Dept of EEE JNTU Kukatpally Hyderabad.

(vijaya.madhavi83@gmail.com, das123tulasiram@gmail.com)

†  
Corresponding Author; S. Vijaya Madhavi, Flat No G1 Srivari Sannidhi Aptmnts Siri Enclave Venkatraya Nagar Nizampet Hyderabad-500090, Tel: 7330813330,corresponding@affl.edu

*Received: 05.03.2019 Accepted:15.04.2019*

**Abstract-** In recent years fuel cells have become prominent as a renewable source of energy to meet the society's energy requirements. These fuel cells need boosting up of the output voltage to interface to utility grid. Isolated Full Bridge Boost converter was mostly used for this purpose in fuel cell systems. Next efficiency and output voltage regulation are the two main aspects of the converter to consider. High efficiency is achieved by reducing the switching losses using zero current switching (ZCS). Then output voltage of the converter is regulated by applying closed loop control techniques like Linear peak current mode control (LPCM) and Non- Linear Carrier Control (NLC). Simulated results of converter with and without ZCS are presented. Losses and efficiencies at various loads are measured. The results show that losses are decreased and efficiency was increased from 62.4% to 96.5% at full load with ZCS technique and output voltage is regulated to 400V with LPCM and NLC control topology.

**Keywords** Fuel Cells; Isolated Boost Converter; Zero Current Switching; Output voltage Controllers.

## 1. Introduction

As fossil fuel reserves are exhausting, environment is polluted due to gas emissions and as energy demands are increasing an emergency situation arises to search for an alternative source of energy. As a result various renewable energy sources have been explored and fuel cells arise as the most efficient alternative energy sources [1] because of its advantages like refuel ability, producing very low emissions, portable in size, little maintenance etc. In spite of these benefits the price of fuel cell is its main constraint [2]. The output voltage of these fuel cells largely varies under variable load conditions and is also very low in magnitude. This low voltage must be raised to peak of the utility to interconnect fuel cells to grid. Therefore dc-dc converters which boost the voltage to the required level are necessary to connect fuel cells to utility loads.

Many models of dc-dc converters are mentioned in the previous survey papers which are

acceptable for fuel cell applications. From the suggested topologies in the literature [3]-[5] Isolated Full Bridge topology was most efficient and acceptable for use in fuel cells. The main advantages of isolated full bridge topology are possibility of applying soft switching techniques, reasonable device voltage ratings, less transistor voltage and current stress, possibility of connecting devices in parallel to achieve desired power levels and high efficiency and galvanic isolation.

Generally two types of converters voltage fed and current fed are proposed in the literature [6]. In fuel cell applications output voltage needed is more than input voltage and also smooth and precise controlling of input/output current is required. Therefore mostly current fed converters are used leading to lower transformer ratio. Standard voltage fed converters need large electrolyte capacitors to handle ripple current and also large transformer turns ratio. So these converters are not used in these applications.

To overcome the problems with hard switching, many soft switching techniques are developed. Depending on application, an IFBC can be operated using zero voltage switching (ZVS) or zero current switching (ZCS) technique. ZVS [7] is used in high voltage applications in which switching losses [8] are important during on period. On the other side in some cases input current needed is high irrespective of input voltage and conduction losses are important. In such applications ZCS is used [9]. In this paper as we are focussing on fuel cell applications with low voltage and high power ZCS [10] topology was chosen. Many types of ZCS techniques using additional switches are mentioned in the literature [11]-[14] which increase switching and conduction losses. But in this paper a simple ZCS technique [15] with no series connected diodes to the switches is implemented to avoid reverse recovery problems.

Under varying load and varying input voltage conditions dc-dc converters must provide regulated dc output voltage. Changes in time, temperature, pressure etc changes the values of the converter components. Applying of negative feedback in the form of a closed loop, regulation of dc voltage can be achieved. Basically two types of controllers, voltage control and current control are in use. Vast majority of dc-dc converters are implemented using current mode controllers because of its advantages [16]. Basic implementation of current control is as shown in figure (1).

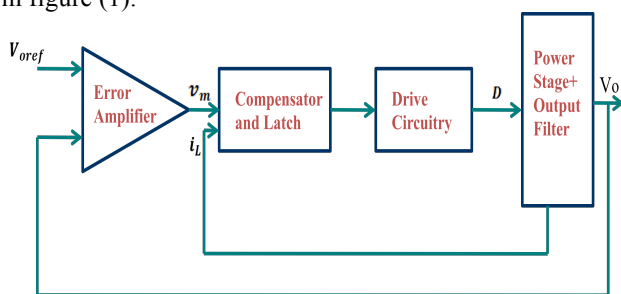


Fig.1. Block Diagram of Current Mode Control

Here output stage is fed with inductor current  $i_L$  and the error voltage output from the error amplifier (known as control voltage)  $v_m$  controls it. This has an extreme effect on a dynamic behaviour of the negative feedback control loop. Peak current control, average current control, non-linear carrier control are some of the techniques using this approach [17]. These control techniques are designed and applied to hard switched isolated boost converter in literature [18]-[19].

Mostly simple PI or PID controllers are applied to soft switched IFBC with a simple dc source in which the transient response is very poor [20]-[23]. So to improve the dynamic response parameters and efficiency of the converter, in this paper a fuel cell sourced current fed ZCS Isolated full bridge boost converter is taken and its operation, steady state analysis are explained in detail. Next two control techniques LPCM and NLC were applied to the converter to control output voltage dynamics. Finally converter is simulated in matlab and regulated output voltage waveforms are presented. Next the switching losses and efficiencies at various loads with and without ZCS are calculated and presented graphically.

## 2. ZCS Isolated Full Bridge Boost Converter (IFBC)

The converter topology is as in figure (2). Transformer leakage inductance and parasitic capacitance are used to attain ZCS conditions which reduce voltage and current spikes on power devices leading to reduced switching losses of converter. Another beneficial feature of this converter is that, secondary side rectifier diodes are operated with ZCS so that they are free from reverse recovery problems.

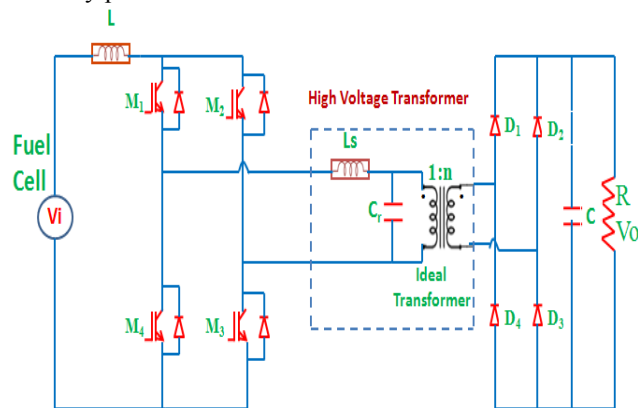


Fig. 2. ZCS Isolated Boost Converter Topology

### 2.1 Operation of ZCS IFBC

From the figure 2  $L_s$  (leakage inductance of transformer or series inductor) and  $C_r$  (parasitic capacitance or resonant capacitor) are the components of resonant tank. Let  $L$  be input inductance large enough. Therefore it shall be considered as dc current source  $I_L$ . The magnetizing current of transformer can be neglected as its magnetizing inductance is very large. The operational waveforms of converter are as shown in figure (3). Here  $T_{zcs}$  is considered as ZCS time of all four primary switches of the converter and is named as overlapping time of all four gate driven signals. Totally ten modes of operation exist for one full cycle. First five modes of operation in a half cycle are symmetrical with next five. Therefore in a half cycle first five modes of operation are explained sequentially and are shown in figure (4)

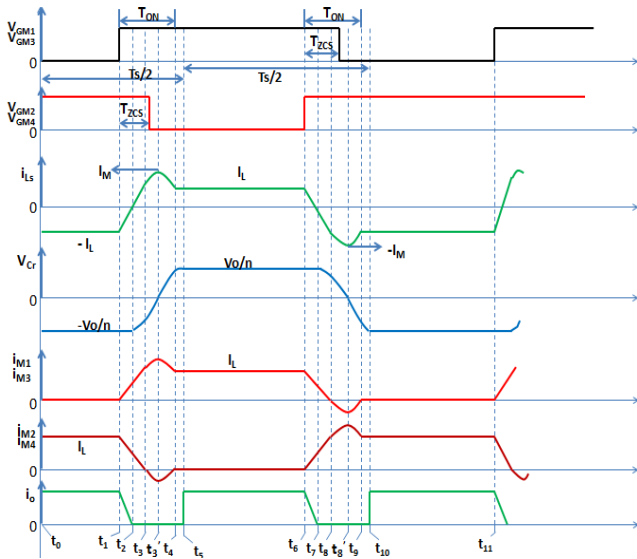
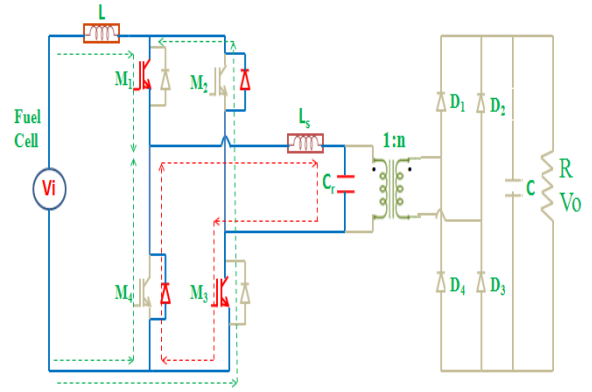
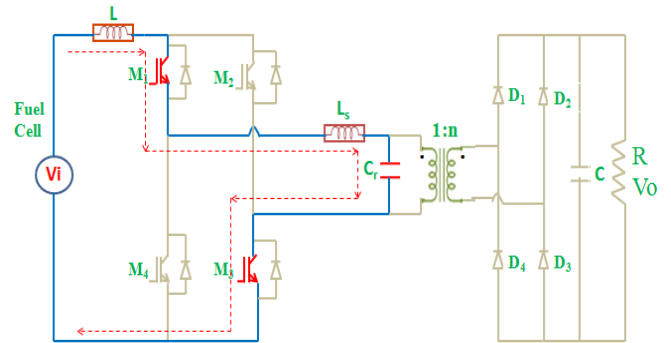


Fig. 3. Operational Waveforms of ZCS IFBC

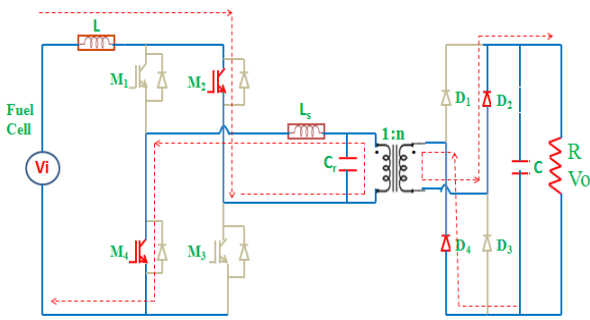


(d) Mode 4

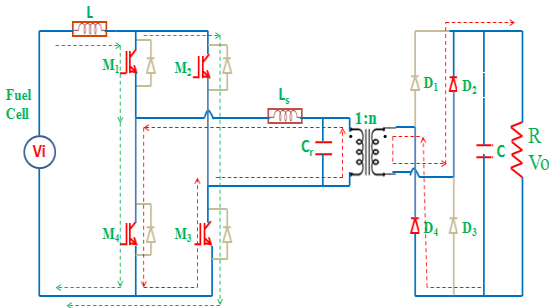


(e) Mode 5

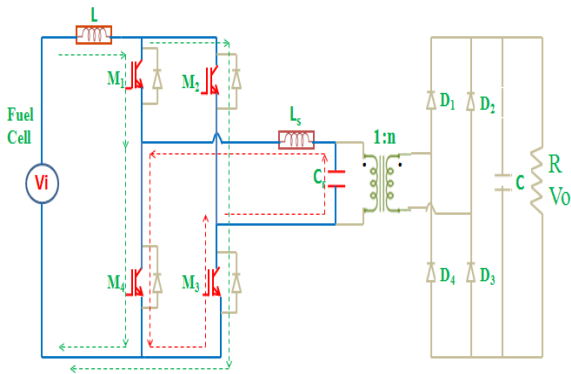
Fig. 4. Modes of Operation of converter



(a) Mode 1



(b) Mode 2



(c) Mode 3

**Mode 1:  $t_0 - t_1$  (Source energy transfer state)**

In this mode of operation switches  $M_2$  and  $M_4$ , diodes  $D_2$ ,  $D_4$  are in operation. This mode is as shown in figure 4 (a). Series inductor current  $i_{L_s}$  is negative and constant. Here input energy is carried to load via high frequency transformer and therefore capacitor voltage is clamped to  $-\frac{V_o}{n}$ . Capacitor voltage  $v_{C_r}$  and output current  $i_o$  are given by equations (1) and (2) respectively. The values of currents through switches are  $i_{M1}=i_{M3}=0$ ,  $i_{M2} = i_{M4} = I_i$  and through diodes  $i_{D2} = i_{D4} = I_i/n$

$$v_{C_r}(t) = -\frac{V_o}{n} \tag{1}$$

$$i_o(t) = \frac{1}{n} I_L \tag{2}$$

**Mode 2:  $t_1 - t_2$  (Boost turn on time,  $L_s$  Energy transfer state)**

At  $t = t_1$ ,  $M_1, M_3$  are turned on. Here all the switches  $M_1 - M_4$  and diodes  $D_2$  and  $D_4$  are in operation as shown in Figure 4 (b). Stored energy in  $L_s$  is transferred to load and  $i_{L_s}$  linearly increases with slope  $\frac{V_o}{nL_s}$ . Currents passing through  $M_2, M_4$  decrease and through  $M_1, M_3$  increase. The related equations are as given below

$$v_{C_r}(t) = -\frac{1}{n} V_o \tag{3}$$

$$i_{L_s}(t) = \frac{V_o}{nL_s}(t - t_1) - I_L \tag{4}$$

$$i_{M_1}(t) = i_{M_3}(t) = \frac{1}{2\pi f_r} \sin^{-1} \left( \frac{nI_L Z_r}{V_o} \right), 0 < 2\pi f_r T_{32} < \frac{\pi}{2} \quad (14)$$

$$\begin{aligned} &= \frac{1}{2} (I_L - (-i_{L_s}(t))) \\ &= \frac{1}{2} \frac{V_o}{nL_s} (t - t_1) \end{aligned} \quad (5)$$

$$\begin{aligned} i_{M_2}(t) &= i_{M_4}(t) \\ &= \frac{1}{2} (I_L + (-i_{L_s}(t))) \\ &= I_L - \frac{1}{2} \frac{V_o}{nL_s} (t - t_1) \end{aligned} \quad (6)$$

$$\begin{aligned} i_o(t) &= -\frac{1}{n} i_{L_s}(t) \\ &= -\left( \frac{V_o}{n^2 L_s} (t - t_1) - \frac{1}{n} I_L \right) \end{aligned} \quad (7)$$

### Mode 3: ( $t_2 - t_3$ ) (Boost turn on time and State of Resonance)

At  $t = t_2$ ,  $i_{L_s}$  becomes zero and diodes  $D_2$ ,  $D_4$  come to off state. Here all switches  $M_1 - M_4$  are in operation as shown in figure 4(c). As resonance exists between  $L_s$  and  $C_r$ , current through  $M_2$  and  $M_4$  decreases, and current through  $M_1$  and  $M_3$  increases. Resonant inductor equation is given by (8). Equations (9) and (10) indicate resonant frequency  $f_r$  and the characteristic impedance  $Z_c$  respectively. At  $t=t_3$ ,  $i_{L_s}$  equals  $I_L$  and current through switches  $M_2$  and  $M_4$  is zero. The currents flowing through the switches are given by equations (11) and (12) and voltage on  $C_r$  is given by (13).

$$i_{L_s}(t) = \frac{V_o}{nZ_r} \sin(2\pi f_r(t - t_2)) \quad (8)$$

$$f_r = \frac{1}{2\pi\sqrt{L_s C_r}} \quad (9)$$

$$Z_c = \sqrt{\frac{L_s}{C_r}} \quad (10)$$

$$\begin{aligned} i_{M_1}(t) &= i_{M_3}(t) \\ &= \frac{I_L + i_{L_s}(t)}{2} \\ &= \frac{1}{2} \left( I_L + \frac{V_o}{nZ_r} \sin(2\pi f_r(t - t_2)) \right) \end{aligned} \quad (11)$$

$$\begin{aligned} i_{M_2}(t) &= i_{M_4}(t) \\ &= \frac{I_L - i_{L_s}(t)}{2} \\ &= \frac{1}{2} \left( I_L - \frac{V_o}{nZ_r} \sin(2\pi f_r(t - t_2)) \right) \end{aligned} \quad (12)$$

$$v_{C_r}(t) = -\frac{V_o}{n} \cos(2\pi f_r(t - t_2)) \quad (13)$$

The duration of this mode can be obtained from equation (7) by substituting  $i_{L_s}(t_3) = I_L$ . Thus

$$T_{32} = t_3 - t_2$$

### Mode 4: $t_3 - t_4$ (Boost turn on time and ZCS period)

Here switches  $M_1$ ,  $M_3$  and body diodes of switches  $M_2$ ,  $M_4$  are in on state. Figure 4(d) shows operation of this interval. As series inductor current  $i_{L_s}$  flow through body diodes of  $M_2$ ,  $M_4$  they come to off state because of ZCS. Similar to that in Mode 3 this period is known as resonant period. At  $t=t_3$ ,  $i_{L_s}$  goes to peak value  $I_M$ ,  $v_{C_r}$  becomes zero. ZCS condition is reached when  $I_M$  becomes greater than  $I_L$ . Using (8) Peak resonant inductor current can be obtained

$$I_M = |i_{L_s}(t)|_{max} = \frac{V_o}{nZ_c} \geq I_L \quad (15)$$

At  $t = t_4$ ,  $i_{L_s}$  equals  $I_L$  and with this resonant period ends. The duration  $t_4 - t_3$  is given by

$$T_{43} = \frac{\pi - 2\pi f_r T_{32}}{2\pi f_r} \quad (16)$$

### Mode 5: $t_4 - t_5$ ( $C_r$ Charge period)

Here switches  $M_1$ ,  $M_3$  are in on state as shown in figure 4(e). Inductor current  $i_{L_s}$  equals  $I_L$  and  $C_r$  is charged by  $I_L$ .  $i_{L_s}$  and  $v_{C_r}$  are given by equations (17) and (18) respectively. The currents flowing through the switches are given by (19) and (20).

$$i_{L_s}(t) = I_L \quad (17)$$

$$v_{C_r}(t) = -\frac{V_o}{n} \cos(2\pi f_r T_{42}) + \frac{I_L}{C_r} (t - t_4) \quad (18)$$

$$i_{M_1}(t) = i_{M_3}(t) = I_L \quad (19)$$

$$i_{M_2}(t) = i_{M_4}(t) = 0 \quad (20)$$

At  $t = t_5$ ,  $v_{C_r}$  becomes  $\frac{V_o}{n}$ . At this instant diodes  $D_1$ ,  $D_3$  are turned on. Duration of this mode is given by

$$T_{54} = \frac{V_o(1 + \cos(2\pi f_r T_{42}))C_r}{nI_L} \quad (21)$$

The half switching period  $\frac{T_s}{2}$  is nothing but the duration from Mode 0 to 5 and is given by

$$t_5 - t_0 = \frac{1}{2} T_s \quad (22)$$

Average output current is given by

$$I_R = \frac{V_o}{R} = \left( \frac{I_L T_{10}}{n} + \frac{1}{2} \frac{I_L T_{21}}{n} \right) 2f_s \quad (23)$$

Where  $f_s$  is the switching frequency. Let us assume that efficiency is  $\eta$ , then the output power is given by

$$P_o = \frac{V_o^2}{R} = \eta P_l = \eta V_i I_L \quad (24)$$

$$\text{Thus } I_L = \frac{V_o^2}{\eta V_i R} \quad (25)$$

The output voltage can now be obtained from equations (22), (23) and (25)

$$V_o = \frac{\eta n V_i}{1 - 2f_s \left( \frac{1}{2} T_{21} + T_{42} + T_{54} \right)} \quad (26)$$

**ZCS Considerations:**

The ZCS condition for the operation of current fed IFBC is that peak inductor current  $I_M$  is more than  $I_L$  while Mode 3 operation. In order to obtain ZCS with input voltage variations, the resonant circuit parameters should be well designed considering variations in input current and input voltage. Therefore condition of characteristic impedance can be derived from (15) and (25)

$$Z_c < \frac{V_o}{n I_{L,max}} = \frac{\eta V_{i,min} R_{full}}{n V_o} \quad (27)$$

Here  $I_{L,max}$  is maximum input current,  $V_{min}$  is minimum input voltage and  $R_{full}$  is equivalent resistance at full load. Generally small value of  $Z_c$  lead to large range of ZCS operation, but power switches are subjected to high current stress. Therefore the time for ZCS operation  $T_{ZCS}$  for the four gate drive signals is limited by

$$T_{31} \leq T_{ZCS} \leq T_{41} = T_{on} \quad (28)$$

**2.2 State Space Modelling of ZCS IFBC:**

In this section, for each mode state space equations are written and then state space model of converter is developed based on averaging [24]. The modelled equations are simplified by taking some presumptions

- Components used are considered to be ideal and lossless.
- Leakage inductance of isolated transformer is included in series inductor.
- Infinitely large magnetizing inductance is assumed.

Steady state equations for each mode of operation in state variable form are written. Next state space averaging is applied on these equations by averaging process [25]. The state variables taken for developing state space model of converter are 1. Input inductor current  $i_L$  2.Series inductor current  $i_{L_s}$  3. Output voltage  $V_o$  and 4. Fuel cell voltage  $V_i$

**Mode 1: ( $t_0 - t_1$ )**

Here switches  $M_2, M_4$  and diodes  $D_2, D_4$  are turned on. Negative current passes through series inductor  $L_s$ . Load receives energy via isolated transformer. Reflected output voltage  $V_o/n$  is blocked by the non-conducting switches  $M_1$  and  $M_3$ . The state space equations in this mode are

$$(L + L_s) \frac{di_L}{dt} = v_i - \frac{v_o}{n} \quad (29)$$

$$i_{L_s} = -i_L \quad (30)$$

$$C \frac{dv_o}{dt} = \frac{i_L}{n} - \frac{v_o}{R} \quad (31)$$

**Mode 2: ( $t_1 - t_2$ )**

Here all switches  $M_1$  to  $M_4$  are in conduction state. Voltage across series inductor  $L_s$  is the reflected output voltage  $V_o/n$ . Now current in it increases linearly, thereby causing linear reduction of currents through switches  $M_2$  and  $M_4$  that are already in conduction. Switches  $M_1, M_3$  start conducting with zero current, decreasing the related turn on loss. The state equations in this mode are

$$L \frac{di_L}{dt} = v_i \quad (32)$$

$$L_s \frac{di_{L_s}}{dt} = \frac{v_o}{n} \quad (33)$$

$$C \frac{dv_o}{dt} = -\frac{i_{L_s}}{n} - \frac{v_o}{R} \quad (34)$$

**Mode 3: ( $t_2 - t_3$ )**

In this mode, increasing or decreasing of currents through all switches occur with same slope as in mode 2. Towards end of this mode, switches  $M_2$  and  $M_4$  are naturally commutated and their currents  $i_{M_2}$  and  $i_{M_4}$  come to zero attaining ZCS. The total current nothing but input current  $I_i$  is carried by switches  $M_1, M_3$ . State equations of mode 2 are applicable to this mode also.

**Mode 4: ( $t_3 - t_4$ )**

Here series inductor current  $i_{L_s}$  further increase with same slope. The anti-parallel diodes of switches  $M_2, M_4$  i.e.  $D_2$  and  $D_4$  conduct. Thus zero voltage continues to appear across commutated switches  $M_2, M_4$  to protect ZCS turn-off condition. This mode ends when currents through transformer and switches  $M_1, M_3$  go to maximum range. This mode must be of very short duration so that maximum current through transformer and switches can be limited, thereby their KVA ratings also. The related state space equations are

$$L \frac{di_L}{dt} = v_i \quad (35)$$

$$L_s \frac{di_{L_s}}{dt} = \frac{v_o}{n} \quad (36)$$

**Mode 5: ( $t_4 - t_5$ )**

Here diodes  $D_1$  and  $D_3$  take over the current immediately which causes reverse polarity of primary voltage of the transformer and current through it decrease. Therefore currents through  $M_1$  and  $M_3, D_2$  and  $D_4$  decrease. When this mode ends, currents in  $D_2, D_4$  become zero and are naturally commutated. The currents flowing through transformer, switches  $M_1, M_3$  goes to  $I_i$ . The state space equations of this mode are

$$L \frac{di_L}{dt} = v_i \quad (37)$$

$$L_s \frac{di_{L_s}}{dt} = -\frac{v_o}{n} \quad (38)$$

For another half cycle also the state space equations can be written correspondingly. Next average of the state equations over a cycle is done. Average value for rate of

change of inductor current  $i_{L_s}$  for a full cycle is zero. Therefore averaged state equation is

$$L_s \left\langle \frac{di_{L_s}}{dt} \right\rangle = 0 \quad (39)$$

Thus state variable  $i_{L_s}$  was neglected in analysis. And also for the ease of analysis the effect of  $L_s$  for variable input inductor current was omitted. Let us notate that  $d_1T_s = t_1-t_0$ ,  $d_2T_s = t_2-t_1$ ,  $d_3T_s = t_3-t_2$ ,  $d_4T_s = t_4-t_3$ ,  $d_5T_s = t_5-t_4$ ,  $d_6T_s = t_6-t_5$ ,  $d_7T_s = t_7-t_6$ ,  $d_8T_s = t_8-t_7$ ,  $d_9T_s = t_9-t_8$ ,  $d_{10}T_s = t_{10}-t_9$ . Now averaged state equations of remaining state variables are as given below

$$L \left\langle \frac{di_L}{dt} \right\rangle = v_i - (d_1 + d_6) \cdot \frac{v_o}{n} \quad (40)$$

$$C \left\langle \frac{dv_o}{dt} \right\rangle = i_{average} - \frac{v_o}{R} \quad (41)$$

Here  $i_{average}$  is average current to output capacitor and load and is given as

$$i_{average} = \frac{i_L}{n} \cdot (d_1 + d_6) \quad (42)$$

Now the equation (41) becomes

$$C \left\langle \frac{dv_o}{dt} \right\rangle = \frac{i_L}{n} \cdot (d_1 + d_6) - \frac{v_o}{R} \quad (43)$$

The switches duty ratio which include the conduction of reverse body diodes is described as

$$d = d_{M1} = d_{M3} = d_2 + d_3 + d_4 + d_5 + d_6 + d_7 + d_8 + d_9 \quad (44)$$

$$d = d_{M2} = d_{M4} = d_1 + d_2 + d_3 + d_4 + d_5 + d_6 + d_7 + d_8 + d_9 + d_{10} \quad (45)$$

Now switches turn-off duration is given by

$$1-d = d_5 + d_6 = d_1 + d_{10} \quad (46)$$

Prolonged duration of anti-parallel diodes of switches is given by

$$d'' = d - 0.5 - \frac{2 \cdot n \cdot i_L \cdot L_s \cdot f_s}{v_o} \quad (47)$$

Here  $f_s$  is switching frequency and  $n$  is turns ratio of the isolated transformer.

Simplified state equations considering new duty cycle ratios are given as

$$L \left\langle \frac{di_L}{dt} \right\rangle = v_i - 2 \cdot (1 - d - d'') \cdot \frac{v_o}{n} \quad (48)$$

$$C \left\langle \frac{dv_o}{dt} \right\rangle = 2 \cdot \frac{i_L}{n} \cdot (1 - d - d'') - \frac{v_o}{R} \quad (49)$$

Now perturbing state variables and input voltage around steady state values, we can write them as follows

$$i_L = I_L + \hat{i}_L, \quad v_i = V_i + \hat{v}_i, \quad v_o = V_o + \hat{v}_o, \\ d = D + \hat{d}, \text{ and } d'' = D'' + \hat{d}''$$

Now with this perturbation the state equations are rewritten as below

$$L \frac{d(I_L + \hat{i}_L)}{dt} = (V_i + \hat{v}_i) - 2 \cdot (1 - D - \hat{d} - D'' - \hat{d}'') \cdot \frac{V_o + \hat{v}_o}{n} \quad (50)$$

$$C \frac{d(V_o + \hat{v}_o)}{dt} = \frac{2 \cdot (I_L + \hat{i}_L)}{n} \cdot (1 - D - \hat{d} - D'' - \hat{d}'') - \frac{V_o + \hat{v}_o}{R} \quad (51)$$

$$(D + \hat{d} - 0.5 - D'' - \hat{d}'') \cdot (V_o + \hat{v}_o) = 2 \cdot n \cdot (I_L + \hat{i}_L) \cdot L_r \cdot f_s \quad (52)$$

By eliminating second order and steady state terms, equations (50), (51) and (52) change to as given below

$$L \frac{d\hat{i}_L}{dt} = \hat{v}_i - 2 \cdot (1 - D - D'') \frac{\hat{v}_o}{n} + 2 \cdot (\hat{d} + \hat{d}'') \frac{V_o}{n} \quad (53)$$

$$C \frac{d\hat{v}_o}{dt} = \frac{2 \cdot \hat{i}_L}{n} \cdot (1 - D - D'') - \frac{2 \cdot I_L}{n} (\hat{d} + \hat{d}'') - \frac{\hat{v}_o}{R} \quad (54)$$

$$(D - 0.5 - D'') \cdot \hat{v}_o + (\hat{d} - \hat{d}'') \cdot V_o = n \cdot L_s \cdot f_s \cdot \hat{i}_L \quad (55)$$

Rearranging equation (55) we can write

$$\hat{d}'' = \frac{(D - 0.5 - D'') \cdot \hat{v}_o}{V_o} + \hat{d} - \frac{2 \cdot n \cdot L_s \cdot f_s \cdot \hat{i}_L}{V_o} \quad (56)$$

Elimination of  $\hat{d}''$  using equation (56) results in

$$L \frac{d\hat{i}_L}{dt} = \hat{v}_i + \frac{4D-3}{n} \cdot \hat{v}_o + \frac{4V_o}{n} \cdot \hat{d} - 4 \cdot L_s \cdot f_s \cdot \hat{i}_L \quad (57)$$

$$C \frac{d\hat{v}_o}{dt} = -\frac{4I_L}{n} \cdot \hat{d} - \left[ \frac{2 \cdot I_L \cdot (D - 0.5 - D'')}{n \cdot V_o} + \frac{1}{R} \right] \cdot \hat{v}_o + \left[ \frac{4 \cdot I_L \cdot L_s \cdot f_s}{V_o} + \frac{2 \cdot (1 - D - D'')}{n} \right] \cdot \hat{i}_L \quad (58)$$

Taking Laplace transform results in

$$(4 \cdot L_s \cdot f_s + L \cdot S) \cdot \hat{i}_L(s) - \frac{4D-3}{n} \cdot \hat{v}_o(s) = \frac{4V_o}{n} \cdot \hat{d}(s) + \hat{v}_i(s) \quad (59)$$

$$\left[ \frac{4 \cdot I_L \cdot L_s \cdot f_s}{V_o} + \frac{2 \cdot (1 - D - D'')}{n} \right] \cdot \hat{i}_L(s) - \left[ \frac{2 \cdot I_L \cdot (D - 0.5 - D'')}{n \cdot V_o} + \frac{1}{R} + CS \right] \cdot \hat{v}_o(s) = \frac{4 \cdot I_L}{n} \cdot \hat{d} \quad (60)$$

Next writing the equations in matrix form

$$\begin{bmatrix} \hat{i}_L(s) \\ \hat{v}_o(s) \end{bmatrix} = [A(s)] \cdot \begin{bmatrix} b_1 \\ b_2 \end{bmatrix} \cdot \hat{d}(s) + [A(s)] \cdot \begin{bmatrix} 1 \\ 0 \end{bmatrix} \cdot \hat{v}_i(s) \quad (61)$$

Where

$$b_1 = \frac{4 \cdot V_o}{n} \quad b_2 = \frac{4 \cdot I_L}{n}$$

$$A(s) = \left[ \begin{array}{cc} 4.L_s.f_s + Ls & -\frac{4D-3}{n} \\ \frac{4.I_L.L_s.f_s}{V_o} + \frac{2.(1-D-D'')}{n} & -\left[ \frac{2.I_L.(D-0.5-D'')}{n.V_o} + \frac{1}{R} + Cs \right] \end{array} \right]^{-1}$$

Matrix A(s) can be expressed as below

$$A(s) = \frac{1}{|A(s)|} \cdot \begin{bmatrix} A_{11} & A_{12} \\ A_{21} & A_{22} \end{bmatrix}$$

Where  $A_{11} = 4.L_s.f_s + Ls$   $A_{12} = -\frac{4D-3}{n}$

$$A_{21} = \frac{4.I_L.L_s.f_s}{V_o} + \frac{2.(1-D-D'')}{n}$$

and  $A_{22} = -\left[ \frac{2.I_L.(D-0.5-D'')}{n.V_o} + \frac{1}{R} + Cs \right]$

$$|A(s)| = -(L.C)s^2 - \left[ \frac{2.L.I_L.(D-0.5-D'')}{n.V_o} + \frac{L}{R} + 4.L_s.f_s.C \right].s - 4.L_s.f_s \cdot \left[ \frac{2.I_L.(D-0.5-D'')}{n.V_o} + \frac{1}{R} \right] + \frac{4D-3}{n} \cdot \left[ \frac{4.I_L.L_s.f_s}{V_o} + \frac{2.(1-D-D'')}{n} \right]$$

**Control to Output Transfer Function**

Now from equation (60) **Controlling Transfer Function** can be attained by substituting  $\hat{v}_i = 0$  as follows

$$\frac{\hat{v}_o(s)}{\hat{d}(s)} = \frac{1}{|A(s)|} \cdot [A_{21} \ A_{22}] \cdot \begin{bmatrix} b_1 \\ b_2 \end{bmatrix} = \frac{N_1(s)}{|A(s)|} \quad (62)$$

Where  $N_1(s) = \frac{4.I_L.L}{n} \cdot s - \frac{8.V_o.(1-D-D'')}{n^2}$

**3. Design of Controllers**

*3.1 LPCM and NLC control methodology*

These types of controllers are based on current control mode theory. In this control mainly the inductor is transformed into a current source thereby removing the inductor performance in the loop. A set value for current is provided by the controller and the loop inside follows this value in each cycle and hence this control can also be called as one cycle control. Why this control is called as linear peak current control because, peak value of inductor current obeys set value and linear relation between the current and off duty cycle ratio. Generally this control has two loops. One is the voltage loop outside which has an error amplifier counteracting dynamic response of output voltage and second a current loop inside which gives compact control on peak inductor current. Sensing of output voltage in this technique can be from a feedback network and the two voltages (reference and output) are compared in a comparator for obtaining the control voltage. Impedance of feedback network is much greater than that of load. Then inductor current sensed and control voltage are compared in modulator to calculate duty ratio

which in turn is changed to output voltage by the power stage.

Inherent sub harmonic oscillations lead to stability problem when the duty ratio of the switches crosses 50% and noise susceptibility. This can soon reset the latch; interrupt the performance of the controller. Therefore the sensed switch current waveform is needed to be filtered by little amount so that the turn on current spike can be discarded which is effected by the diode stored charge. To overcome this adding a substitute ramp for the controller makes better the noise immunity of the circuit. So generally to keep away from instability problem, control scheme is altered with addition of artificial ramp to sensed inductor current waveform [26] but result is it increases circuit complexity. So to make the control scheme easy an approach known as quasi-steady-state is generally used. With this technique, a simple equation is solved in the modulator and thereby switch duty ratio [27] is obtained. Equation consists of sensed current (i.e. switch current average for NLC) on one side and opposite side is carrier wave obtained by computing the result of voltage loop outside.

The main distinction between NLC and LPCM controllers is by producing a proper carrier, NLC controller executes average current control in contrast peak current controller produces distinct wave in order to apply the actual concept of peak current mode control. Figure (5) shows the Schematic form of representation of the LPCM and NLC controllers

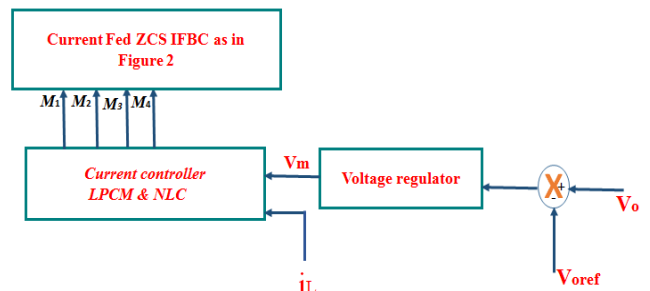


**Fig. 5.** Block Diagram of LPCM and NLC Controllers

The non-linear carrier control applies average current mode control. Therefore the generalised control objective for NLC is

$$f(i_L)_{NLC} = i_{L,avg(T)} = \frac{1}{T} \int_0^T i_L dt \quad (63)$$

And in LPCM the function is

$$f(i_L)_{LPCM} = i_{Lp} = i_L(dT). \quad (64)$$

Where  $i_{Lp}$  is peak inductor current.

This current in one switching period goes to its peak at when the switch reaches to the end of on time  $dT_s$ .

**4. Simulation Results with ZCS and Controllers**

The ZCS Current Fed IFBC was constructed and simulated in MATLAB Simulink. The open loop simulation diagram is as shown in figure (6). The converter is simulated by taking a 6KW 45V fuel cell as the input source. Based on

the theory and principles stated in section 3 the controller blocks for LPCM and NLC and their carrier waves are generated in MATLAB using transfer function derived from equation (62) which are as shown in figures (7) and (8) respectively. From the detailed design considerations with reference to [25] the converter parameters are as shown in table 1. The switching losses of the converter measured at various loads with and without ZCS are as shown in table 2. The efficiencies calculated at various loads of converter with and without the ZCS are shown in figure (9) graphically. Figure (10) shows ZCS operation of switch  $M_2$ . Finally regulated output voltage waveforms of converter with LPCM, NLC controllers are shown in figures (11) and (12) respectively.

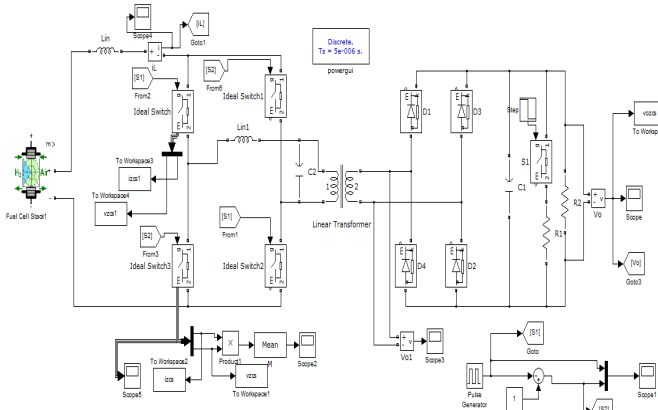


Fig. 6 MATLAB Simulation Block Diagram of ZCS IFBC

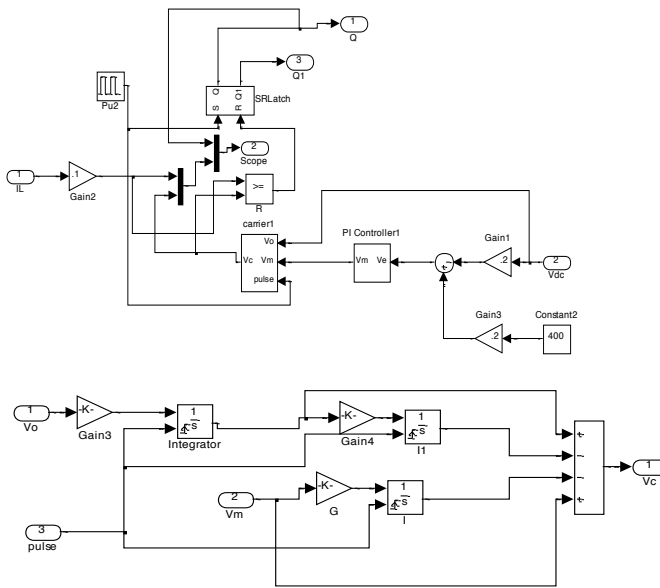


Fig. 7 LPCM Controller and Carrier Generation Blocks

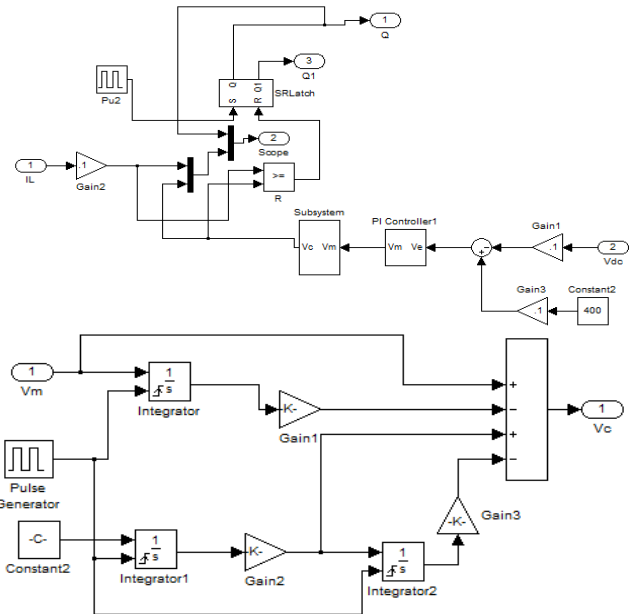


Fig. 8 NLC Controller and its Carrier Generation Blocks

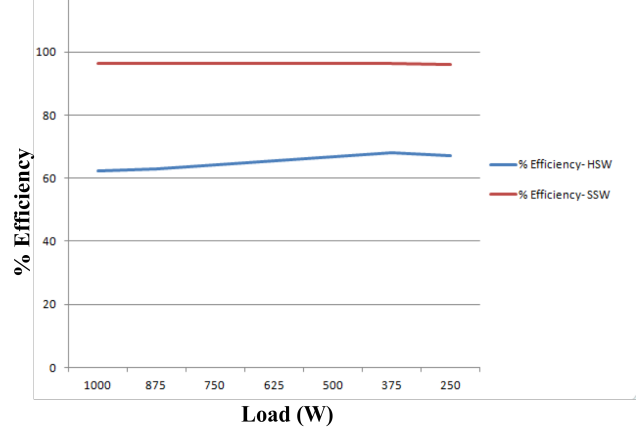


Fig.(9) Efficiency of the ZCS IFBC at Various loads

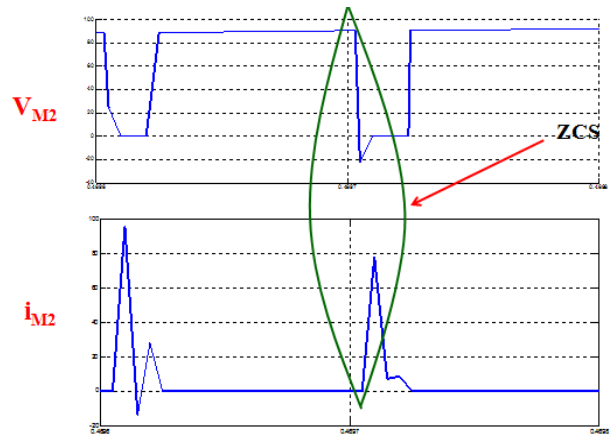


Fig. 10 Simulated Zero Current Switching waveforms of Switch  $M_2$

**Table 1** Design Specifications of IFBC

Specification	Value	Specification	Value
Output Power	1kw	Output Capacitor C	470 $\mu$ F
Input Voltage Vi	Fuel cell (6kw ,45V DC)	Load Resistor R	(400*400)/Po ohms
Output Voltage Vo	400V	Transformer voltage turns ratio	45:400
Input Inductor L	2.5mH	Switching Frequency	10KHz
Series Inductor Ls	0.16 $\mu$ H	Resonant or Parasitic Capacitor Cr	0.838 $\mu$ F

**Table 2** Switching Losses Measured and Efficiency Calculation

Load Power (w)	Losses Hard Switching (w)Per switch	Losses Soft Switching (w) Per switch	Input-Hard Switching	Input- Soft Switching	% Efficiency-HSW	% Efficiency-SSW
1000	151	9.28	1604	1037.12	62.4	96.5
875	128.75	8.4	1390	908.6	63	96.4
750	104.5	7.43	1168	779.72	64.3	96.2
625	82.42	6.1	954.68	649.4	65.5	96.3
500	62	4.86	748	519.44	66.9	96.3
375	43.75	3.65	550	389.6	68.2	96.3
250	30.6	2.68	372.4	260.72	67.2	95.9

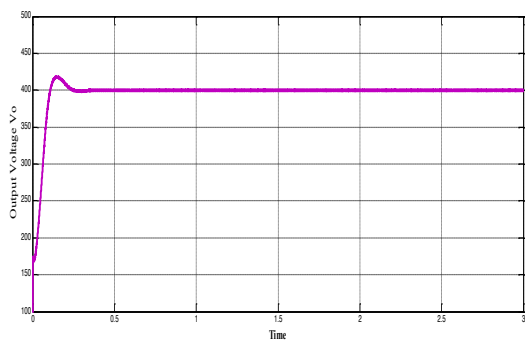


**Fig.11.** Output voltage of ZCS IFBC with LPCM Controller

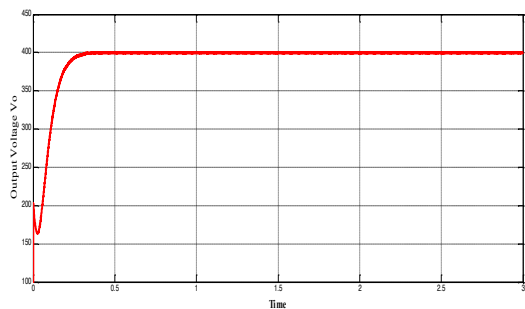


**Fig.12.** Output voltage of ZCS IFBC with NLC Controller

**5. Discussion of Results**

From the results obtained we can see that by using zero current switching losses are decreased and thereby efficiency of the converter is increased from 62.4% to 96.5% when compared to hard switching. High efficiency is obtained at full load. Next by applying LPCM and NLC controlling techniques the output voltage is regulated to 400V. From the transient response it can be observed that with LPCM controller better response is achieved as the settling time is only 0.25s compared to NLC which is almost 0.4s. These controllers designed for fuel cell can be applied to converter with any dc source

**6. Conclusion**

In this paper a fuel cell sourced current fed zero current switching (ZCS) isolated full bridge boost dc-dc converter for low voltage fuel cell applications was presented and implemented in closed loop configuration. The operation and modelling of the converter topology was also presented in detail. The switching losses and efficiencies of the converter at various loads were measured with and without ZCS condition and efficiency curves were drawn at various loads. From the simulated results it can be shown that switching losses of converter with ZCS decrease and efficiency of converter is increased from 62.4% to 96.5% with ZCS. High efficiency is obtained at full load condition. Next LPCM and NLC controlling techniques were applied to converter topology to regulate

output voltage. Simulated results show that output voltage is regulated to 400V and LPCM control topology is better than NLC.

## References

- [1] Amar Nath Mishra, Vijay Kumar Manjhi, Dr. Archana Soni and Dr.K.Sudhakar “OPPORTUNITIES AND CHALLENGES FOR FUEL CELLS IN INDIA” *International journal of Advanced Research in Science and Engineering*, Vol.No.5, Issue No6, June 2016.
- [2] Recent advances and challenges of fuel cell based power system architectures and control – A review Vipin Das, Sanjeevikumar Padmanaban, Karthikeyan Venkitesamy, Rajasekar Selvamuthukumar, Frede Blaabjerg and Pierluigi Siano *Renewable and Sustainable Energy Reviews* 73 (2017) 10–18 journal homepage: [www.elsevier.com/locate/rse](http://www.elsevier.com/locate/rse)
- [3] A. Emadi, S. S. Williamson, and A. Khaligh, “Power electronics intensive solutions for advanced electric, hybrid electric, and fuel cell vehicular power systems,” *IEEE Trans. on Power Electronics*, 2006, pp. 567-577.
- [4] A. Emadi, K. Rajashekar, S. S. Williamson, and S. M. Lukic, “Topological overview of hybrid electric and fuel cell vehicular power system architectures and configurations” *IEEE Trans. on Vehicular Technology*, 2005, pp. 763-770.
- [5] A New System-Level Model for the Fuel Cell in a Strategic Context Gomer Abel Rubio, W. Agila 2018 International Conference on Renewable Energy Research and Applications (ICRERA)
- [6] Haruka Hatsuyado and Nobukazu Hoshi “A High Boost Ratio DC-DC Converter for Low Voltage Fuel Cell” 2014 International Conference on Renewable Energy Research and Applications (ICRERA)
- [7] G. Moschopoulos and P. Jain, “Single-stage ZVS PWM full-bridge converter,” *IEEE Trans. Aerosp. Electron. Syst.*, vol. 39, no. 4, pp. 1122–1133, Oct. 2003.
- [8] Mohammadjavad Baei\*, Mehdi Narimani†, and Gerry Moschopoulos “A New ZVS-PWM Full-Bridge Boost Converter” *Journal of Power Electronics*, Vol. 14, No. 2, pp. 237-248, March 2014
- [9] P.Parvathy and Dr.N.Devarajan “Simulation and Implementation of Current-Fed Full-Bridge Boost Converter with Zero Current Switching for High Voltage Applications” *IJCSI International Journal of Computer Science Issues*, Vol. 9, Issue 3, No 3, May 2012
- [10] Yu Zhang, Chushan Li, Zhifang Cao and David Xu “Soft-Switching Single-Stage Current-Fed Full-Bridge Isolated Converter for High Power AC/DC Applications” 9th International Conference on Power Electronics-ECCE Asia June 1 - 5, 2015
- [11] I. Gerald Christopher Raj, P. Soundar Rajan, G. Praveen Raj, J. Anjel “A Study and Hardware Implementation of Enhanced Isolated Boost DC-DC Converter with the Reduced Number of Switches” *International Journal of Innovative Technology and Exploring Engineering (IJITEE)* ISSN: 2278-3075, Volume-8 Issue-5S March, 2019
- [12] Aravind Murali, Mr.Benny.K.K, Mrs.Priya.S.P “A HIGHLY EFFICIENT ISOLATED DC-DC BOOST CONVERTER” *International Journal of Scientific Development and Research (IJS DR)* September 2016 Volume 1, Issue 9
- [13] Shelas Sathyan, Hiralal Murlidhar Suryawanshi, Bhim Singh, Chandan Chakraborty, Vishal Verma, and Makarand Sudhakar Ballal “ZVS–ZCS High Voltage Gain Integrated Boost Converter for DC Microgrid” *IEEE TRANSACTIONS ON INDUSTRIAL ELECTRONICS*, VOL. 63, NO. 11, NOVEMBER 2016
- [14] Efficiency Improvement of Isolated Bidirectional Boost Full Bridge DC-DC Converter Satoshi Ikeda, Kazuhiro Kajiwara, Kazuki Tsuji, Fujio Kurokawa 2018 International Conference on Renewable Energy Research and Applications (ICRERA)
- [15] Ahmad Mousavi, Pritam Das and Gerry Moschopoulos “A ZCS-PWM Full-Bridge Boost Converter for Fuel-Cell Applications” 978-1-422-2812-0/09/\$25.00 ©2009 IEEE
- [16] Mr.S.Dhanasekaran, 2Mr.E.Sowdesh Kumar, 3Mr.R.Vijaybalaji “Different Methods of Control Mode in Switch Mode Power Supply- A Comparison” *International Journal of Advanced Research in Electrical, Electronics and Instrumentation Engineering* Vol.3, Issue 1, January 2014
- [17] Fujio Kurokawa, Shusuke Maeda and Yudai Furukawa “Analysis of Digital Peak Current Control DC-DC Converter” 2014 International Conference on Renewable Energy Research and Applications (ICRERA)
- [18] Pratapsinh G. Parmar , Urvashi D. Patel , Manish S. Patel “Closed Loop Control of Bi-Directional DC-DC Converter” *INTERNATIONAL JOURNAL OF INNOVATIVE RESEARCH IN ELECTRICAL, ELECTRONICS, INSTRUMENTATION AND CONTROL ENGINEERING* Vol. 4, Issue 2, February 2016
- [19] M.Sai Krishna Reddy , K.Chandana, U.Chenchu Lakshmi “Design, Analysis and Simulation of High gain Isolated Front end DC-DC converter for Interfacing Fuel cell to DC micro grid application” *International Journal of Pure and Applied Mathematics* Volume 114 No. 9 2017.
- [20] S.Ajitha and N.Kalaiarasi “Implementation of Full-Bridge Current-Fed Resonant Boost Converter using PIC microcontroller” 2010 *International Journal of Computer Applications* (0975 – 8887) Volume 1 – No. 7
- [21] Mouncef Arazi, Alireza Payman, Mamadou B Camara, Brayima Dakyo “Control of Isolated DC/DC Resonant Converters for Energy Sharing between Battery and Supercapacitors” 2018 International Conference on

Renewable Energy Research and Applications  
(ICRERA)

- [22] L. Navinkumar Rao , Sanjay Gairola , Sandhya Lavety, Noorul Islam “Design of DC-DC Boost Converter with Negative Feedback Control for Constant Current Operation” International Journal of Power Electronics and Drive System (IJPEDS) Vol. 8, No. 4, December 2017, pp. 1575~1584
- [23] G. Seshagiri Rao, S. Raghu, N. Rajasekaran “Design of Feedback Controller for Boost Converter Using Optimization Technique” International Journal of Power Electronics and Drive System (IJPEDS) Vol. 3, No. 1, March 2013, pp. 117~128
- [24] J.-F. Chen, R.-Y. Chen, and T.-J. Liang, “Study and implementation of a single-stage current-fed boost PFC converter with ZCS for high voltage applications,” in *IEEE Trans. on Power Elec.*, Jan. 2008, vol. 23, no.1, pp. 379-386.
- [25] Ren-Yi Chen, Tsorng-Juu Liang, *Member, IEEE*, Jiann-Fuh Chen, *Member, IEEE*, Ray-Lee Lin, and Kuo-Ching Tseng “Study and Implementation of a Current-Fed Full-Bridge Boost DC–DC Converter With Zero-Current Switching for High-Voltage Applications” *IEEE TRANSACTIONS ON INDUSTRY APPLICATIONS*, VOL. 44, NO. 4, JULY/AUGUST 2008
- [26] Hidenori Maruta, Fujio Kurokawa, Junya Sakemi, Akihiro Nakamura, Hiroyuki Osug “A New Prediction Based Digital Control for DC-DC Converter” International Journal Of Renewable Energy Research , IJRER Vol.1, No.2, pp.76-85, 2011
- [27] Y. Massaoudi, D. Elleuch, D. Mehdi, T. Damak, and G. Hashim, “Comparison between non linear controllers applied to a DC-DC boost converter,” International Journal of Innovative Computing, Information & Control, vol. 11, no. 3, pp. 935–947, 2015.